Dynamic Regulation of Growth and Physiology of Microbes under Complex Changing Conditions

Somenath Bakshi*[,1,2], Emanuele Leoncini*[,1], Charles Baker[3], Silvia J. Cañas-Duarte[1], Burak Okumus[1,3], and Johan Paulsson[1]

*These authors contributed equally
Correspondence should be addressed to:
S.B. (somenath.bakshi@eng.cam.ac.uk) and J.P. (Johan_Paulsson@hms.harvard.edu)

[1]Department of Systems Biology, Harvard Medical School, Boston, Massachusetts, USA,
[2]Department of Engineering, Cambridge University, Cambridge, UK
[3]Biophysics Program, Harvard University, Boston, Massachusetts, USA,
[4]Current Address: ArcherDX, Saint Louis, Missouri, USA

ABSTRACT

As microbes deplete local resources and transition from exponential to stationary phase they can change greatly in size, morphology, growth and expression-profiles. These responses can also vary importantly between individual cells, as shown by population snapshots. However, it has been difficult to track individual cells along the growth curve to determine the progression of events or correlations between how cells enter and exit dormancy. We have developed a platform for tracking >10^5 parallel cell lineages in dense and changing cultures, independently validating that the imaged cells closely track the batch population. This provides a microcosm of bulk growth with exceptional resolution and control, while enabling conventional bulk assays on the same culture. We used the platform to show that for both *Escherichia coli* and *Bacillus subtilis*, growth changes from an 'adder' mode in exponential phase to a mixed 'adder-timer' entering stationary phase, and then a near-perfect 'sizer' upon exit – creating broadly distributed cell sizes in stationary phase – and rapid return to narrowly distributed sizes upon exit. By high-throughput tracking of single cells as they enter and exit stationary phase, we further show that the heterogeneity in entry and exit behavior has little consequence in regular wake up from overnight stationary phase but can play important role in determining population fitness after long periods of dormancy or survival against antibiotics.

INTRODUCTION

Bacteria in natural environments go through periods of starvation and stress punctuated by the arrival of fresh nutrients that then get depleted again as cells grow and divide[1,2]. Many mechanisms have therefore evolved to help cells weather busts and exploit booms[3–5]. Traditionally these have been studied by inoculating cultures of stationary phase cells into fresh media and following them along the growth curve back into stationary phase[6–8]. However, batch assays consider average properties of cells, while single cell studies have revealed great cell-to-cell heterogeneity during stress[9,10]. This could be a mere side effect of saturated pathways displaying less heterogeneity than sub-saturated pathways, making all cells 'happy the same way but unhappy in different ways', but could also be an adaptive response to maximize inclusive fitness in uncertain times[11], e.g. by making a small fraction of cells persistent to drugs[12]. Either way, because the heterogeneity is so substantial and so profoundly changes the fate of stressed cells, effective studies of bacterial responses to stress and starvation should ideally monitor individual cells as they enter and exit stationary phase.

This is challenging for several reasons: *First*, though it is straightforward to sample cultures at different times, either manually[13] or with microfluidic automation[14], this only provides snapshots of the heterogeneity. The dynamics of fluctuations are also important, since rapidly changing heterogeneity is easily time-averaged by affected processes while slowly changing heterogeneity can effectively establish cell states. Snap-shots provide little information about the progression of events or the connection between heterogeneity and growth[15]. *Second*, studies of heterogeneity are hard to interpret or reproduce unless local conditions are tightly controlled, which is particularly challenging to achieve when components become limiting and conditions keep changing. *Third*, many important outliers in stress response and stationary phase, e.g. persister cells, can be exceedingly rare, making it important to sample large numbers of cells. Some microfluidic devices boost

effective throughput by accumulating data over long time windows[16], but experiments during changing conditions, e.g. along the growth curve, must instead rely purely on high-throughput parallel imaging.

Here we present a microfluidic platform based on the 'mother machine' design[17] that addresses all these challenges. We monitor the physiology and gene-expression of individual cell lineages over multiple consecutive growth curves in and out of stationary phase, while ensuring that the cells imaged behave quantitatively as the cells in a connected batch culture that can be simultaneously sampled. This provides a microcosm of bulk growth in the microfluidic device, with exceptional resolution and control, while also enabling conventional bulk assays on the same culture. Our current throughput of >100,000 cell lineages in parallel, imaging 10^8 cells per day, each every few minutes, is high enough that we observe spontaneous persisters without using special mutants[18,19]. The setup also works at very high cell densities, e.g. $OD_{600}\approx10$, both for the Gram-negative *Escherichia coli* and Gram-positive *Bacillus subtilis*. In a first application we probed the size-regulation principles of *E. coli* during entry into and exit from stationary phase, and demonstrated trade-offs between the behaviors entering and exiting stationary phase.

RESULTS

A platform for studying single cells along a growth-curve

Several imaging platforms allow for long-term tracking of cells, and some can run almost indefinitely[17,20]. However, only a handful of studies have actually required ultra-long-term imaging (see e.g. Norman *et al.*[16]), and the main difference between platforms instead lies in how tightly they can control local conditions, which translates into data quality. Platforms like the 'mother machine'[17] where individual cells grow and divide in narrow trenches that are fed diffusively by orthogonal flow-channels, have emerged as the methods of choice in this regard, and can, if designed and operated properly, achieve exceptional spatial and temporal uniformity. However, to our knowledge all studies that used this setup have considered balanced growth of cells in constant, dilute medium – in stark contrast to microbiology experiments more broadly, despite the fact that time-lapse imaging of single cells is arguably most sorely needed as cells enter or exit starvation[21–23]. Thus even the most reliable methods for controlling local growth environment has so far been limited to a small subset of the conditions of interest in microbiology.

The challenge is that fluid handling for non-viscous and unchanging liquids is very different from the handling of dense and changing cell cultures needed to study stationary phase cells or ecosystems. Also, in changing systems, it is important that the cells imaged track cells in the batch culture of interest. Specifically, it is easy to starve cells on any platform by simply letting media run out, but for reproducibility and interpretability, the imaged cells need to be starved the same way as in a standard bulk experiment.

We therefore built a system that can flow dense cultures of cells from a conventional batch experiment into a mother machine type of microfluidic device, (Fig. 1a-b), such that cells loaded in the mother machine will experience the same environment as cells in the batch, whether a gradual depletion of nutrients or sudden stresses, and therefore undergo the same physiological changes[24]. Since cells can be retained in the device for hundreds of generations, this allows us to observe how individual cell lineages pass through multiple rounds of entering and exiting stationary phase (Supplementary Movie 1). The process is fully automated, has virtually zero dead volume and provides near-perfect timing about when the media changes occur (Supplementary Information section 1). The optical density is monitored continuously using a custom OD-meter, in series with the flow path, to align any part of the observed single-cell data to the bulk OD (see Supplementary Information section 2 and 7).

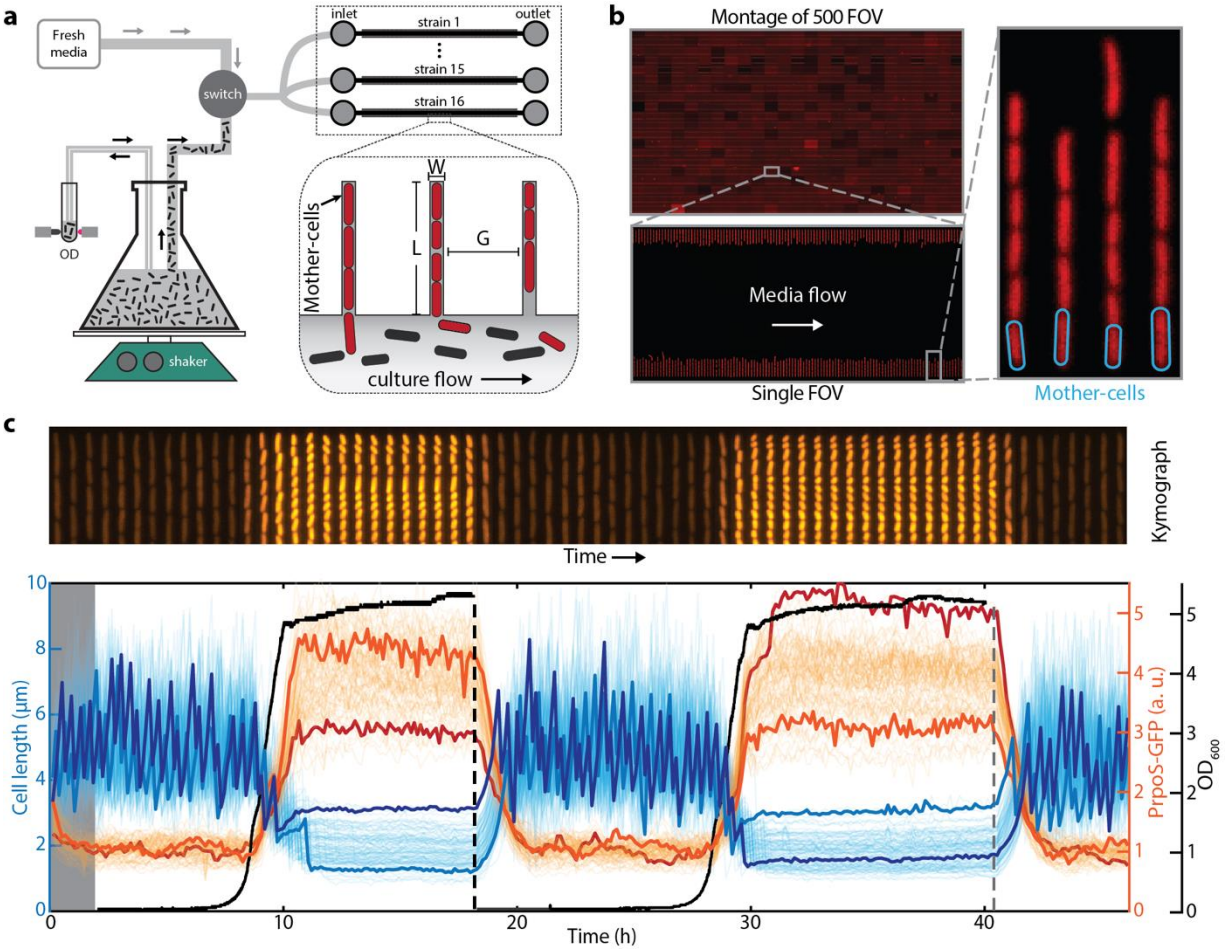

Fig. 1| Accurate high-throughput measurement of cell-growth physiology and gene-expression along growth-curve. (a) A simplified schematic depicting the growth curve platform. The platform is based on the mother machine microfluidic device (right of the panel) in which cells under observation are grown in trenches (shown in red) while liquid media is pumped through an orthogonal flow channel. To observe growth dynamics, we flow actively growing bulk culture into the mother machine device while continuously observing its Optical Density (OD). As the bulk culture flows past (black cells) the red cells in the device (red) respond synchronously with the batch culture. At any point, a switch can be made to flow fresh media, allowing us to observe cells return to optimal exponential growth. The dimensions (W, L, and G in the inset) of the mother machine were highly optimized to meet the demanding requirements associated with flowing dense cultures through the flow channels. (b) The optimizations made to the mother machine design have greatly improved the throughput. We can image up to 16 strains in parallel, with imaging of 705 fields of view (FOV), each containing 186±1 lineages, in under 5 minutes, giving a throughput of 131,072 ($= 16 \cdot 8{,}192$) lineages imaged every 5 minutes often for multiple days. We show a montage 500 such FOVs in the top left corner. Note the range of intensities present in the individual FOVs in the montage of FOVs has been increased for visualization purposes. (c) (TOP) A kymograph showing a single lineage of cells in a trench expressing a fluorescent RpoS transcriptional reporter as it goes through two consecutive rounds of growth-curve as depicted in the panel below. (BOTTOM) Here we show 80 single-cell traces, from a single field of view, of RpoS expression and cell-size as cells enter and exit from two consecutive rounds of stationary phase. Two cell size traces and two expression traces are highlighted and illustrate high variability between the two rounds of stationary phase. The high-throughput measurements of each property allow us to measure accurate distributions of expression level and cell sizes at any time-point along the growth-curve.

This allows us to correlate specific states of nutrient depletion and bulk properties with their corresponding single-cell phenotypes at any time. However, the mother machine was so far designed and used for exponential growth under constant condition, and a series of technical challenges must be overcome to ensure that the cells in mother machine are representative of cells grown in the flask whose physiology and environment in changing over time:

First, as opposed to a simple syringe of fresh media that can be kept next to the microfluidic device, shaking batch cultures must sometimes be much larger to allow for bulk assays, and must be separated from the microscope to prevent vibrations from affecting image acquisition (Supplementary Information section 3). To ensure that cells in the flow-path do not undergo changes during transit from the culture to the microfluidic device, the flow paths must be short and carefully designed to prevent bio-film formation, non-uniform temperatures, exposure of cells to surfaces other than inert tubing, and cross-contamination between the fresh-media and culture paths. After extensive trial and error, our setup (see Supplementary Information section 1) achieves that in a way that can be easily adopted for any batch culture and any microscopy setup.

Second, shaking cultures contain large amounts of bubbles, which can greatly change the flow in the microfluidic chip and thereby greatly change local conditions. This required the incorporation of custom-designed automated bubble-traps, to prevent the transmission of bubbles to the mother machine (see Supplementary Information section 2). Third, though low-density cultures can be flown through most microfluidic devices, at high ODs it is necessary to optimize the dimensions to prevent clogging from dense cultures while maintaining proper diffusive feeding and retention of cells for experiments that typically last multiple days. This is particularly challenging because the cell volumes also change greatly during the experiment (*E. coli* MG1655 can change 15-fold in volume along the growth curve, and MC4100 even more than that). We therefore evaluated approximately 540 combinations of widths, heights, and lengths of the narrow trenches where cells grow and divide, (L, W, and G in Fig. 1a) to find near-optimal parameters for each growth condition (Supplementary Information section 4). All of the experiments described in this paper were performed in Neidhardt defined medium[25] (rich: EZ-rich defined medium, poor: Mops buffered medium; recipes for both media are provided in the Supplementary Information section 18). Both the rich and poor media were adjusted to desired osmolarity (0.28 Osm) with NaCl[26]. The experiments with *B. subtilis* were performed with a modified version of the EZ-rich defined medium published by the Weisshaar group[27].

Fourth, since it is no longer possible to simply accumulate data over time, as under constant conditions in regular mother machine experiments, we systematically optimized the chip to increase parallelism and statistical sampling. We determined the smallest inter-trench distance that did not introduce significant fluorescent bleed-through artifacts from point-spread function overlap (Supplementary Information section 5), and further optimized the dimensions of the feeding channels and overall layout to maximize the number of cells imaged while still maintaining effective feeding and high image quality (Supplementary Information section 6). This e.g. included designing the flow-channel layout of traditional mother machine to have trenches on both sides of the flow channel. This allowed us to observe 186 individual trenches in every Field of View at 40x magnification (Fig. 1b), while scanning 705 FOVs every 5 minutes for a single color and every 7 minutes for two-color imaging. The platform records cell size, morphology, and changes in gene-expression levels as cells traverse the growth-curve, while tracking either 8,192 lineages from each of 16 different strains or 122,880 ($= 15 \cdot 8{,}192$) lineages of a single strain (Supplementary Information section 6), imaging every few minutes over the course of multiple days as cells experience multiple rounds of entry and exit from stationary phase (see Supplementary Information section 6). Because each trench contains multiple cells, this allows us to observe on the order of 100 million cell divisions per experiment – enough to observe many rare events and to accurately measure distributions of properties, while also correlating multiple events along the growth-curve. To illustrate a typical experiment, Fig. 1 shows the layout of the device and time-lapse images of cells entering and exiting stationary phase while expressing a transcriptional reporter of the master regulator of stress response, RpoS (Prpos-GFP).

Finally, our goal is not merely to subject cells to some unknown level of stress and starvation, but to observe cells along virtually the same growth curve as in the connected batch culture. We therefore first tracked the dynamics of cell-size and the expression of an *rpoS* transcriptional reporter (Prpos-GFP) upon entry to stationary phase. As the OD of the batch culture goes through a diauxic shift, the bulk growth-rate drops momentarily, and both the cell length and Prpos reporter fluorescence respond synchronously (Fig. 2a, Supplementary Movie 2). This indicates that the bulk dynamics are impacting cells in the microfluidic device with minimal delay and in the expected ways, i.e. population doubling time, individual cell-size and rpoS expression as a result of increased stress. The specific growth-rate of cells displays a sharp drop during this time, mimicking the bulk growth rate, but displaying much richer behavior that is difficult to infer from the bulk OD data (see Supplementary Information section 8).

To further ensure that the cells in the mother machine are quantitatively representative of cells in the batch culture, even at the level of single cell fluctuations, we sampled cells from batch for immediate microscopy, and compared to the cells growing in the mother machine at the same time points. We compared the cell length and reporter activity of the Prpos-GFP reporter strain from the device at different time-points along the growth-curve to small aliquots taken from bulk culture at corresponding times and imaged via snapshots (Fig. 2b). For the entry to stationary phase, cells were aliquoted from the batch culture at multiple time-points during growth and imaged under agar pads. The cells were imaged within 5 minutes of being removed from batch culture and care was taken to keep cells at 37°C throughout. The magnitude and dynamics of the Prpos expression-dynamics and the cell length matched closely to the results for the mother cell, see Fig. 2c. The slight discrepancy of PrpoS dynamics in stationary phase was demonstrated to come from a slight PSF artefact in the agar-pads (see Supplementary Information section 5 and 8) where some of the light emitted by a cell will be allocated to its neighbors – another reason to use mother machine setups instead of two dimensional microcolonies. For exit from stationary phase, high statistical sampling is difficult with traditional microscopy since the cultures are so dilute. We therefore used a second microfluidic device which makes it possible to take snap-shots of cells from batch cultures in very high throughput[28]. Similar to what was observed for entry, the results from this control closely matched that observed with the platform (Fig. 2d). These orthogonal controls within the same experiment, i.e., for the same time-points of the same culture, demonstrate the ability of our platform to capture single cell dynamics in conventional batch culture.

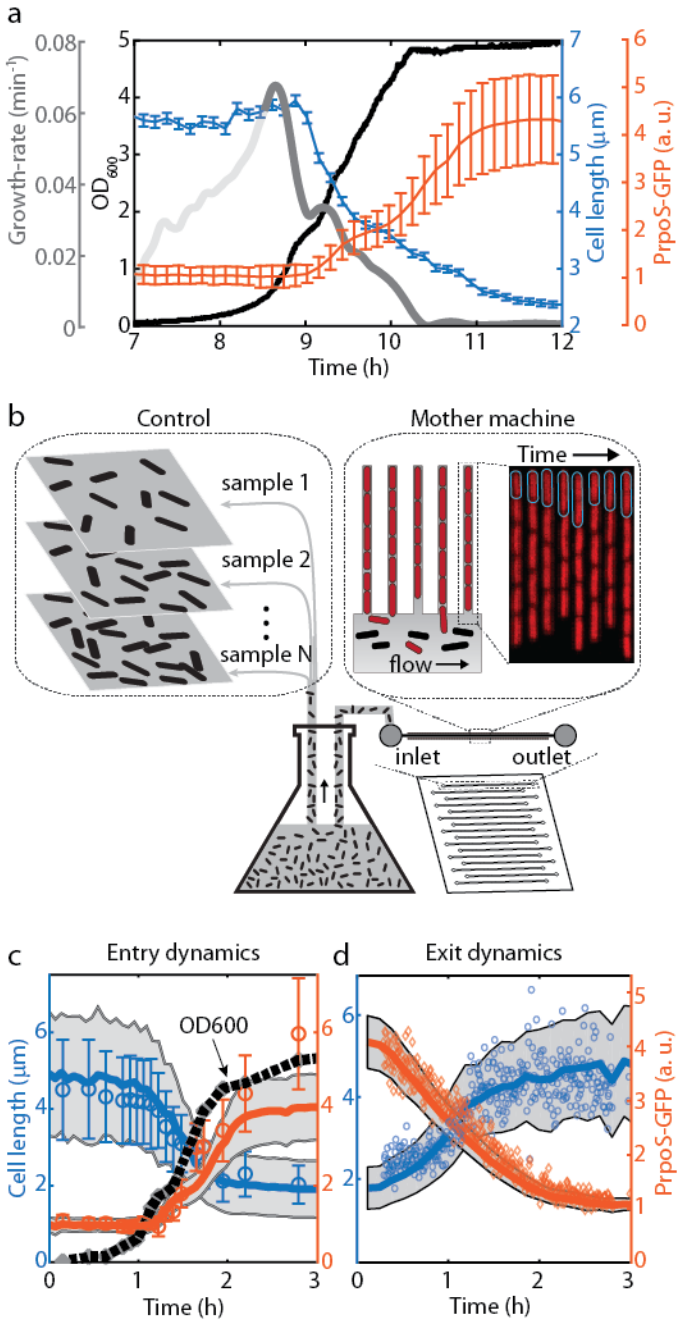

Fig. 2| (a) The bulk dynamics observed in the flask are synced with the dynamics of the mother machine. When the optical density (black), goes through an inflection point -- valley in bulk growth rate (grey), representing here the rate of change in OD per minute – there is a synchronous drop in the cell length (blue) and an increase of RpoS transcriptional activity (orange) of the cells in the mother machine device. (b) To determine how well the cells in the mother machine trenches mimic the cells grown in bulk, snapshots were taken of cells grown in the growth chamber flask. During entry (c) and exit (d) from stationary phase the measured cell length and RpoS intensity match that found with the mother cells in the growth chamber platform, with snapshots of cells sampled from bulk. The average trend from the cells in mother-machine are plotted as solid lines (blue – cell length, orange – RpoS transcriptional activity). In (c) simple agar pad snapshots (blue circles – cell length, orange circle – RpoS) are compared with measurements in mother-machine during the entry to stationary phase. OD600 (black) of the culture is shown in [0, 7.2] range as in both y-axis. During exit, the snapshots were acquired with the MACS microfluidic device[28], which allows very dilute cultures present during exit from stationary phase to be observed (d). The value from individual cells are plotted as blue circles (length) and orange diamonds (RpoS). The shadowed region and the errorbars corresponds to +/- 1 standard deviation.

Size regulation during entry and exit from stationary phase

The ability to quantitatively track growth and expression dynamics with single-cell resolution as bacteria enter and exit dormancy could provide important information about virtually any process in the cell. We first applied it to study how cells regulate their size along the growth-curve, as they enter stationary phase from exponential phase and exit upon the introduction of fresh media. Specifically, previous analyses have characterized where cell size regulation falls with respect to three simple mechanisms: adders, sizers and timers, that capture how individual cells in a population respond to being born smaller or larger than average. The adder mode is characterized by a constant addition of cell volume each division, the sizer mode is characterized by division at a fixed volume threshold, and timers are characterized by division after a fixed time interval[29], all with some variation but independently of the size of the newborn cell. Virtually all studies on size control to our knowledge have concluded that cells, including several bacteria, archaea, and eukaryotes, closely follow the adder model of growth control, in a wide range of environments from fast growth to starvation[30–33]. However, though size regulation in *E. coli* has been evaluated in a large number of conditions, including starvation, it has to our knowledge not yet been tested for the gradual entry into and exit from stationary phase which is so often encountered by growing populations.

We used a 100x apodized phase objective, imaging 2,215 lineages of *E. coli* MG1655 at one-minute intervals for over 30 consecutive hours to observe growth dynamics during balanced growth and then entry and exit from stationary phase. The 100x apodized phase imaging using the oil objective and one-minute sampling rate reduces our throughput but provides extremely fine resolution and accuracy for the size-regulation study. We first computed the specific growth rate (rate of increasing cell mass), and the splitting rate (inverse of time between cell divisions) (Fig. 3a). The details of this calculation are provided in supplementary material section 14. In balanced growth, the observed average specific growth rate (0.043 per minute) and splitting rate (0.044 per minute) are both similar to the estimated bulk growth rate (0.043 per minute) (Supplementary Information section 7 and section 14). The CV in specific growth rate (0.053) was approximately three times lower than the standard deviation in the splitting rate (0.16), in agreement with previous literature[34,35]. After the period of balanced growth, we observed an initial sharp drop in the specific growth-rate followed by a brief increase. The specific growth-rate drops and partially recovers couple more times, and then steadily decline to zero, as expected as cells go through diauxic shift but then deplete all nutrients (Fig. 3b-c, Supplementary Information section 8). The splitting rate by contrast is much more refractory through the diauxic shift all the way into stationary phase (Fig. 3c). This mechanism allowed cells to produce daughters with ever decreasing sizes as cells enter stationary phase, causing the average cell size to drop rapidly (see Supplementary Information section 10). A similar phenomenon was previously observed in bulk experiments during nutrient downshifts, and attributed to 'rate-maintenance'[36], caused by the fact that cells can only split into two daughter cells once initiated rounds of replications are completed. However, whatever the mechanism, this suggests that cells change their cell-size regulation as they enter stationary phase from exponential phase.

To determine which mode of the three—timer, sizer, or adder—best described the observed size-regulation in different phases of the growth-curve, we examined the Pearson correlation coefficient (C) between cell size at birth (L_{birth}) and division (L_{div})[29]. In the "timer" model C = 1, since L_{birth} and L_{div} are near-perfectly correlated, whereas in the "sizer" strategy C = 0, where the size at division is fixed (L_{div} = constant), thus yielding no correlation between L_{birth} and L_{div}. The adder represents a compromise between the other two growth modes with C=0.5 giving a strong but not perfect correlation between L_{birth} and L_{div}. We first confirmed that our cells used an adder-like mechanism during balanced exponential growth (C=0.54), as expected (Fig. 3d). For non-balanced conditions, the analysis must be done carefully to avoid confounding effects from an average that changes systematically in time. Thanks to the high throughput, we could avoid such effects by only comparing cells born in the same brief time interval, analyzing their subsequent growth as a function of their varying initial size (see Supplementary Information section 9). Consistent with the rate-maintenance phenomenon, where cells maintained a constant division time even as they start to grow more slowly, this revealed that size control becomes a mix of an adder and timer (C=0.8, Fig. 3e). During exit from stationarity the cells started out with widely varying sizes but still underwent the first division at a uniform size, i.e., with almost pure sizer dynamics (C=0.09, Fig. 3f). We further calculated the slopes of the linear fit of division length vs. birth length, observing slopes of 0.998 for exponential phase, 1.23 for entry to stationary phase and 0.06 for exit from stationary, consistent with the proposed adder, mixed adder-timer and sizer models respectively. We note that while the cells act as near-perfect sizers in the first division during exit, they then immediately switch back to adder mode

from the second division onwards (Fig. 3g). The size regulation strategies observed in the rich growth medium (EZRDM) at 37°C were also consistent with measurements at different temperatures (30°C and 40°C) (Supplementary Information Table S12).

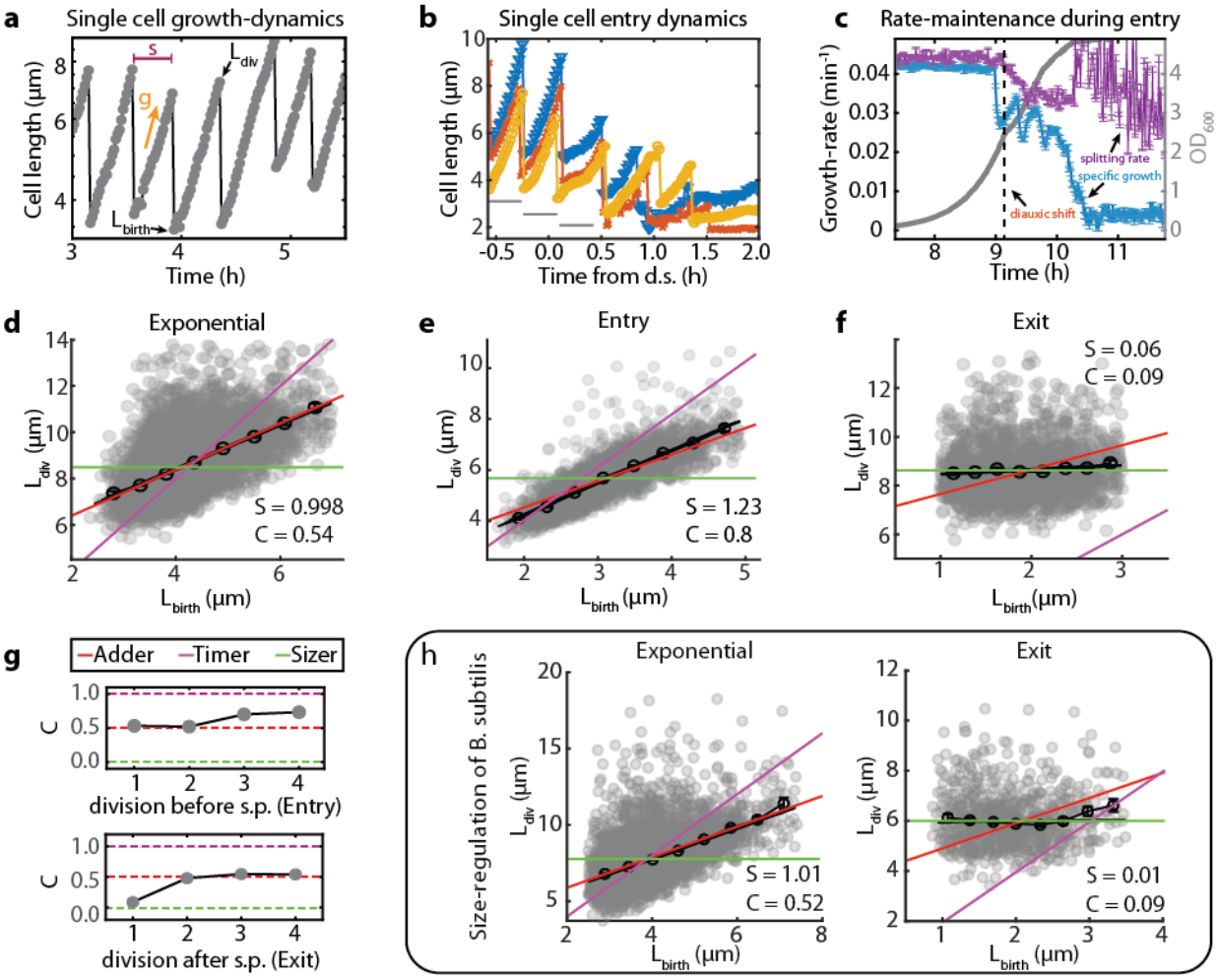

Fig. 3| Cell size regulation during entry and exit from stationary phase reveals novel control principles. (a) Cell length of a single bacterium is plotted (log-scale) with time showing exponential growth of size at single cell-level and division occurring every 20 minutes. Both the specific growth-rate (g) and splitting-rate (s) can be computed from a single trace (see Supplementary Information section 14). Since the data is collected every 1 min, we get a high-resolution estimation of the size at birth (L_{birth}) and size at division (L_{div}). (b) Cell lengths of three representative bacteria is shown as they enter stationary phase after passing through diauxic shift (d.s.). (c) The average splitting rate and specific growth-rate of the population are plotted in terms of number of doublings per minute at each time point of the experiment relative to the diauxic shift time-point. During the entry to stationary phase, the cell splitting rate (purple line) is changing gradually through the diauxic shift (dotted line), but the natural specific growth rate (blue) drops precipitously. (d) Correlation between cell lengths at birth and division are plotted during exponential growth phase. Grey circles are data from single division events, and black circles are binned along the x-axis. Theoretical lines for the adder, timer, and sizer models are shown as red, purple, and green lines. (e) Correlation between cell lengths at birth and division are plotted during the entry to stationary phase (1.0 hour from diauxic shift at OD 1.5). (f) Correlation between cell lengths at birth and division are plotted during the exit from stationary phase. (g) Investigating the size-regulation mode for every division cycle reveals the dynamics of switch between different modes. Top –The correlation coefficient between lengths at birth and division for the last four divisions before cells stop dividing shows that cells switch to the timer mode (purple line) of size regulation in the last two division before entering stationary phase. Bottom - Cells are perfect sizer (green) during the first division as they exit stationary phase (C ~0), but are already in adder mode (red line) in the second division and after. (h) Size-regulation strategies of *B. subtilis* cells along the growth-curve: Left - Correlation between cell lengths at birth and division are plotted during exponential growth phase; Right - Correlation between cell lengths at birth and division are plotted during the exit from stationary phase.

To explore whether such regulation strategies are shared across different types of bacteria, we performed similar measurements on the Gram-positive model organism *B. subtilis*, which is separated from *E. coli* by a billion years of evolution. The details of the single-cell growth-curve experiments of *B. subtilis* cells are provided in Supplementary Information section 16. In remarkable similarity to *E. coli* cells, the cells of *B. subtilis* also displayed adder mechanism of size regulation during exponential phase (C=0.52) as previously observed, while following a near-perfect sizer mechanism (α=0.09) for exit from stationary phase (Fig. 4c-d). Analysis of the size-regulation during entry to stationary phase for the *B. subtilis* strain is complicated by lysis of cells and consequent growth-resumption of cells in the same trench (Supporting Movie 3) This is reminiscent of the 'cannibalistic' behavior observed in bacillus strains during starvation[37], and detailed analysis of this behavior is out of the scope of this paper. However, we found that *B. subtilis* cells also display 'rate-maintenance' during the entry to stationary phase, which suggests we should expect them to follow timer dynamics during this phase.

Many different mechanistic models have been found to be consistent with the 'adder' mode of size control, from titration mechanisms to various forms of control connected to chromosome replication[38,39]. Our additional observations may also be consistent with more than one model as well, but by demonstrating three distinctly different modes in three different situations, we believe that, combined with more systematic analyses of various mutants, this kind of experiments will help distinguish between possible mechanistic models[40,41].

Consequences of cell size variation in stationary phase

Sizers, adders and timers are expected to create very different overall heterogeneity in cell volumes, where pure timers fail to compensate for deviations in size and accumulate great variation, while sizers could accurately correct size deviations and adders are intermediate between the two. Partly as a consequence of the mixed adder-timer growth dynamics during entry to stationary phase, the distribution of cell volumes in stationary phase is therefore much broader than in exponential growth (CV about 0.26 in stationary phase compared to 0.16 in exponential growth). The sizer mechanism at exit from stationary phase then causes a rapid return to narrowly distributed volumes (CV=0.15).

However, some of the size variation in stationary phase also reflects the fact that a subpopulation of cells can undergo several more divisions than others (Fig. 4a). Simply being more numerous can be highly advantageous since individual cells can explore the world independently, and have a higher overall chance of finding new resources. However, those smaller cells would also exit from stationary phase with less cellular resources. Understanding the consequences of heterogeneity therefore requires tracking of cells as they enter and exit from stationary phase in multiple rounds, to compare advantages and disadvantages.

We found that during an overnight in stationary phase (~8 hours), cells display great heterogeneity in division patterns both when entering and exiting, but in a negatively correlated manner such that the net effect is to display virtually no variation in the total number of divisions (Fig. 4b). For example, during a time window around the stationary phase, where every cell had at least one division before entry and after exit (Fig. 4a), the largest 10% of cells in stationary phase, that divide the least as they enter stationary phase, on average go through 3.14 ± 0.07 doublings during a time window, whereas the smallest 10%, which divide the most as they enter stationary phase, similarly double 3.26 ± 0.05 times. The same principle was found under all media conditions tried, and demonstrates the importance of tracking individual cells. This observation – which is made possible by tracking cells over time – could in fact help explain why such great heterogeneity in either phase (entry/exit) can exist, since, at least in the short term, there appears to be no substantial advantage or disadvantage of either strategy.

We then considered longer periods of stationary phase to investigate the consequence of such heterogeneity of entry-exit strategies. After one week of starvation, we tracked exit from stationary phase upon addition of a poorer defined medium (MOPS buffered medium, MBM)[25]. This by contrast revealed a great net growth disadvantage of cells that divide more times as they entered in stationary phase, where e.g. none of the smallest 10% of cells began growth within 10 hours of adding fresh media, but 85% of the largest 10% of cells started to divide in that time window (Fig. 4c-d). Larger cells, which spend less resources on increasing their numbers in the entry to stationary phase, can thus reap a substantial growth advantage after long periods of dormancy. Indeed, the fraction of cells that started dividing in the observation window (10 hours) was a monotonically increasing function of the cell size in stationary phase (Fig. 4d).

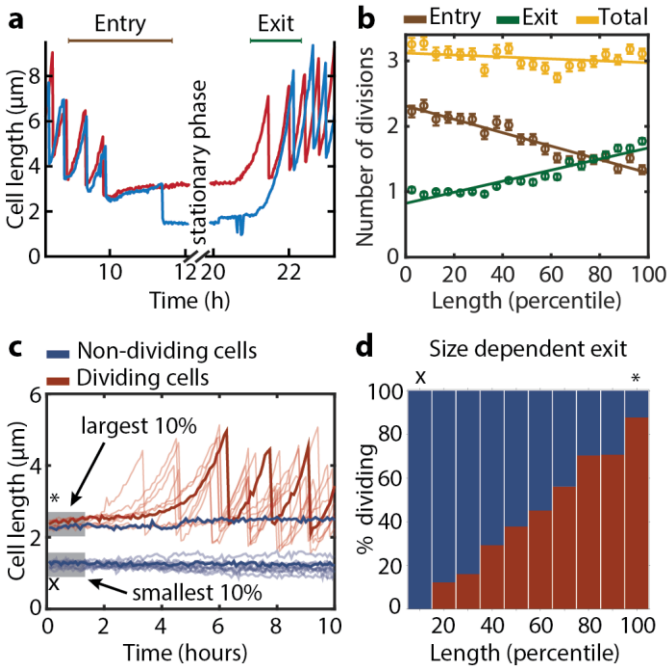

Fig. 4| Stationary phase length distribution and survival of deep stationary phase (a) Two sample traces shown in blue and red highlight the differing number of divisions performed during entry and exit for small vs. large stationary phase cells respectively. (b) The number of divisions performed during entry (brown), exit (green) and in total from entry through exit (yellow) are plotted vs. stationary phase cell size binned by percentile. The mean values are plotted with error bars (SEM) and a linear regression line is fit to these points. (c) Cells were subjected to a stationary phase lasting 1 week before being provided with fresh media. Cell length time traces for 10 example cells that exited from deep stationary phase are plotted in translucent red, a sample trace is overlaid in opaque red. The same is shown in blue for a sample of 10 cells that did not begin dividing within 10 hours of receiving fresh media. (d) The percent of cells for a given cell size that began dividing within 10 hours is shown in red and the percent that never began dividing are shown in blue.

These results raise the question of why all cells do not stop dividing earlier, to ensure viability after stress. One reason may be the simple advantage in being more numerous, but we also considered if smaller cells could be more prone to persist in the presence of antibiotics[42]. A small fraction of cells can become persistent towards antibiotic treatment after experiencing starvation, a phenomenon that is called 'triggered persistence'[19]. It has so far been hard to monitor persisters cells over time, both because many platforms cannot ensure local uniformity under stress and because persistence usually is limited to a very small fraction of cells ($<10^{-2}$). However, our combination of tightly controlled local conditions and extreme imaging throughput enables us to directly track a large number of natural persisters, without relying on mutants which may change not only the frequency of persisters but also their properties[18]. Because cells in our setup occupy dedicated growth trenches, cells at the end of each trench are also shielded from competition, which enables long-time monitoring of slow growers that would otherwise be lost by dilution in bulk cultures.

Using this approach we tracked ~80,000 individual mother-cells that were kept in stationary phase for 36 hours. The cells were then treated for 3 hours with fresh media containing a lethal dose of ampicillin (100 μg/ml, 10x MIC, 99.7% mortality), an antibiotic known to specifically target actively dividing cells[43]. To determine which cells return to an actively growing state, antibiotic-free rich growth medium was then flowed past the cells 3 hours post antibiotic treatment for an additional 12 hours. We found that a majority of cells exiting stationary phase during this 3 hours period were killed by the antibiotic (grey traces in Fig. 5b) treatment, but that some persister cells remained dormant through the antibiotic treatment, and then switched into a non-persister growing state once the antibiotic was removed (see example in Fig. 5a, Supplementary Movie 4). We observed a total of 214 such persister cells, at a relative frequency of $3x10^{-3}$, (orange, Fig. 5b), consistent with our own bulk measurements (see Supplementary Inforation section 15) and previous reports[42].

Comparing the properties of cells that did or did not turn into persisters showed a striking trend: the cells that were smaller as they enter stationary phase were much more likely to turn into persisters (Fig. 5c). Indeed, of the 10% smallest cells, a fraction of 3% turned into persisters, while none of the 45,000 cells that were larger than the average cell produced a single persister. This also provides what may be an important new clue in the search for persister-creating mechanisms, by showing that the decision to become a persister is at least partly determined already when cells enter stationary phase, such that cells that divide into smaller cells are the only ones that – at least under our conditions – form persisters.

Thus, we observe a clear tradeoff: prolonged stays in stationary phase confer great advantages to cells that stop dividing early if cells exit stationary phase without drugs, but instead a great disadvantage if cells exit stationary phase with drugs. This may suggest that there is selective pressure behind the great heterogeneity observed in the entry to stationary phase: on short time-scale there is no disadvantage to such heterogeneity, but for longer periods of stationary phase – where it is increasingly difficult to anticipate the environment under which the cells will wake up – that variation can be necessary to ensure that at least some cells survive.

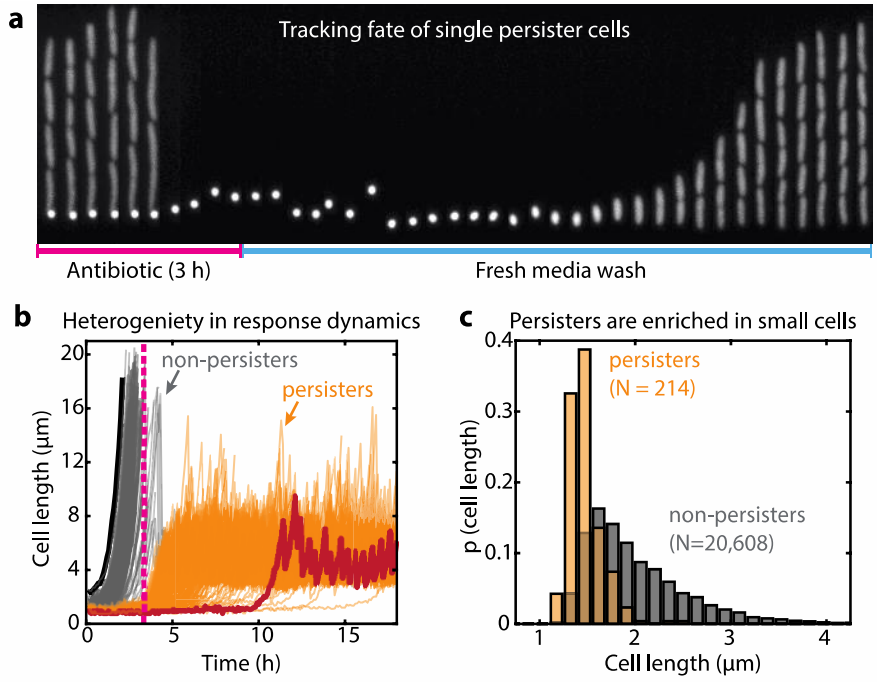

Fig. 5| Size distribution in stationary phase and survival during antibiotic treatment. (a) Kymograph showing a trench containing persister mother cell, during antibiotic treatment and recovery. (b) 200 sample traces of persister cells (orange) and non-persisters (cells that chain and die during Amp treatment) are shown. The largest and smallest cell in the population are highlighted in black and red. Larger cells tend to exit quickly and are therefore vulnerable to Amp treatment, whereas smaller ones exit stationary phase later and survive. (c) Distribution of cell sizes in stationary phase for cells that eventually become persisters in stationary phase is compared to the overall population, where each population has been independently normalized.

DISCUSSION

The success of microbes in natural environments depends on their ability to exploit booms and weather busts[44]. To some extent this in turn relies on the ability to sense and adapt to environmental changes. For example, we observe 'rate-maintenance'* in the entry to stationary phase, where cells maintain the generation times from balanced exponential growth for several more divisions than they maintain their mass growth rates, which causes cells to get smaller rapidly. This can be advantageous by creating a larger number of 'exploring units' that could separately venture into new niches and suggests that cells are able to track depletion in nutrient. However, in many cases it is not possible to adapt fast enough. For example, cells may not survive the sudden arrival of drugs unless they are already in a drug-tolerant state, and unless they are immediately ready to grow and divide they may instead be unable to take advantage of fresh resources before these are depleted by competing cells. Clonal populations could therefore benefit from hedging their bets and ensuring that individual cells are prepared for different future environments[45,46].

Great phenotypic heterogeneity has indeed been observed both as cells enter and exit stationary phase[21,47]. However, both the temporal patterns of heterogeneity and their consequences for survival and propagation have been hard to analyze due to the limitations of existing methods[15]. The method we present here enables us to track lineages entering and exiting stationary phase with precise enough control of local environments to make the results straightforwardly interpretable, over long enough time window, and with high enough throughput to observe key outliers. The first proof-of-principle applications already reveal important insights into the dynamics of bacteria under such complex changing conditions. First, we found that *B. subtilis* and *E. coli* qualitatively change their size regulation with growth phase, which then dictates the variability in cell size. Specifically, as many others before us[30–35], we found that cells act as 'adders' in exponential phase, in the sense of adding a volume that is uncorrelated with the birth-size. However, we then found that cells change control in the entry to stationary phase to become closer to 'timers' where division occurs after a specific time since

the last division, and almost perfect 'sizers' in the first division upon exit from stationary phase in the sense of dividing at a critical volume regardless of the size of the newborn cells. The timer dynamics contributes to the large variation in stationary phase cells and the sizer dynamics ensures a fast return to much smaller size variation in exponential phase. Interestingly cells use sizer mode for only the first division after exiting from stationary phase, and switch to 'adder' mode immediately after the first division from exit. The observation that growth control displays a distinct pattern of adders, timers and sizers, may in turn restrain models more than the observation of adders alone. Specifically, many models of growth control invoke replication patterns, and as described above, those patterns are different in entry and exit from stationary phase[39,40]. However, dividing more times without additional protein production also causes changes in the levels of division proteins, which also have been invoked in explanations of growth control[41,48]. More detailed models of how these processes change during entry into and exit from stationary phase may thus help discriminate between various hypotheses, especially if also analyzing how various mutants control growth as they enter and exit stationary phase.

Second, by tracking individual cell lineages through multiple rounds of growth and starvation we not only observe the heterogeneity at any given growth phase, but also trade-offs between them. We believe the rate-maintenance phenomenon underlies the shift to timer-mode observed in cells during the entry to stationary phase. This causes cells to get smaller rapidly and, because some cells stop dividing later than others, contributes to the heterogeneity observed in size. This in turn has consequences for how cells exit stationary phase. After short periods of starvation, cells that entered stationary phase smaller accordingly delay their divisions upon exit. By comparing divisions before and after we find that the two effects closely offset each other: despite great heterogeneity in how cells both enter and exit, the total number of divisions is virtually constant. Thus, the heterogeneity appears to have little impact on net growth under those conditions. The rate maintenance mechanism may then be advantageous by creating a larger number of 'exploring units' that could separately venture into new niches. After longer periods of dormancy, however, we see very different patterns: the smallest cells are then by contrast much less likely to survive, or greatly delay growth if they do survive, but those small cells are also the only ones that became persisters and transiently survive antibiotics.

The molecular mechanisms behind both growth control and persisters have been notoriously controversial, with many studies making credible claims for competing hypotheses[49]. Though we do not pinpoint any mechanisms here, we believe our phenotypic observations and methodology could help future studies converge on molecular explanations. First, the observation that the cells that become persisters divided more times during entry into stationary phase shows that whatever mechanism is behind the persisters can be triggered already at that time. For example, the tendency to continue to divide even as mass growth is slowed or stopped has been linked to replication, where cells prioritize completing replication forks and placing chromosomes in separate cells. Extended replication in some cells could in turn deplete resources. Alternatively, persisters could be created by the growth and division process itself, e.g. due to fluctuations to low concentrations that arise when cells sub-divide an already low protein content into multiple small cells, which perhaps does not change the average concentration but should create more heterogeneity between cells. Indeed, we observe that only some of the small cells become persisters.

In conclusion, many processes in cells display interesting heterogeneity, and virtually every process could display much richer behavior along the growth curve than in balanced growth alone. Our method transforms the microfluidic platform 'mother-machine' into a microcosm of bulk growth with exceptional resolution and control, while enabling conventional bulk assays on the same culture. Because the cell culture can contain virtually any mix of cells, our method could equally be used to study individual cells in ecosystems, e.g. microbiome studies. We therefore believe the ability to track the growth, death and expression patterns of individual cells over time in dense, complex and changing cultures – potentially containing whole ecosystems – could be transformative in many areas of microbiology.

METHODS

Strain construction: Strain BO37 was used in the bulk culture flask. It was built by P1 transducing *glmS::*P_{RNAI}-mCherry$_{1-11}$-mKate-T1 terminator-FRT Kan FRT::pstS allele into MG1655 as described in Okumus *et al.*[28]. For all the strains used in the mother machine, we used the MG1655 7740 background with ΔmotA. The strain SB8 was used for the phase contrast imaging experiments depicted in Fig. 3b-g and Fig. 4a-b is the background strain for all the other strains containing transcription reporters used in this study. SB8 was constructed by a P1 transduction from the Keio collection strain CGSC#:9565, ΔmotA743::kan into MG1655 and flippase was used to remove the kanamycin resistance[50]. For fluorescent segmentation marker, we made a fluorescent version called SB7, by P1 transducing *glmS::*P_{RNAI}-mCherry$_{1-11}$-mKate-T1 terminator-FRT Kan FRT::pstS into this SB8 strain. We made 16 different strains containing transcription reporters for different processes, including the PrpoS reporter, by integrating the transcription reporters constructed by Uri Alon's group[51] into the SB7 strain. To rigorously check if the ΔmotA was introducing any artifacts to our measurements, we compared our results with ΔfliC, which also renders the cell nonmotile, and finally compared with the MG1655 6300, which is much less motile than 7740 version and found that the results were identical.

Mother machine chip preparation: The construction of the wafer and selecting dimension of the single-cell trenches are described in detail in the Supplementary Information. Here we give a brief description of how we made the mother machine devices once we have the wafer ready. To prepare the PDMS for the mother machine chips, dimethyl siloxane monomer (Sylgard 184) was mixed in a 10:1 ratio with curing agent, defoamed and then poured onto the silicon wafer. This was then degassed for 1h using vacuum, and then cured at 95 °C for 1 hour. Individual mother-machine chips were cut out of the PDMS mold and holes were created for the inlets and outlets using a biopsy puncher (0.75 mm). Coverslips were cleaned by sonication in KOH followed by sonication in DI water and then bonded to the feature side of the mother-machine chips using oxygen plasma treatment (30 seconds at 50 W and O_2 pressure set to 170 mTorr) followed by incubation at 95 °C for at least 1 hour. Chips were bonded the day before being used in experiments.

Loading cells in the mother machine chips: There are two types of experiments described in this article and they use two different types of mother machine devices (see Supplementary Information section 16). In general, 16 different strains can be loaded into the 16 different lanes of the device type 1. We used 16 pairs of gel-loading tips for loading those lanes and centrifuge the chips to load the cells into the trenches that are orthogonal to the loading lanes. The high-throughput experiments involve a single strain to be loaded in a mother machine device where 15-lanes are connected via a continuous snake-like feeding channel. In this case, the overnight culture is concentrated 10x before loading into the device. The chip is then spun at 4500 rcf in a benchtop centrifuge for 2 min, using a custom-built holder. The centrifugal force rapidly loads the cells in the narrow-trenches. The dense culture from the feeding channel was washed quickly with fresh growth-medium before starting the image acquisition.

Description of growth curve platform: Cells are grown in a 500 mL baffled bottom flask (ChemGlass) that is being shaken at 220 rpm on an orbital shaker with magnetic clamps (Benchmark Scientific Orbi-Shaker Jr). A set of peristaltic pumps (Langer Instruments) circulates the culture to and back from a custom-designed inline OD-meter (see Supplementary Information section 2). Another set of pumps takes the culture to the mother machine device loaded on the microscope stage and flows through it. In order to make sure that throughout this entire process cells are maintained at 37°C, to avoid any cold or heat shock, we house the entire systems of pumps, valves, and the shaker with culture flask in a home-built incubator. The incubator was constructed using T-slot framing and acrylic, then heated with an OEM resistive heater and fan. The temperature of the incubator is constantly monitored in two places using a custom microcontroller solution and a data-logging thermometer. This incubator houses multiple peristaltic pumps, solenoid valves and a culture shaker. The tubing containing the culture and fresh media go out of this incubator into the incubator that houses the microscope. The path between the two incubators is kept insulated using an insulating duct the inside of which is actively kept warm using fans that blows the 37°C air from the incubator.

Description of a growth-curve experiment: Before any experiment is run with the platform, an automated system is used to wash the entire media and culture tubing path. The wash consists of ~40 minute wash with

20% bleach, followed by 40 minute wash with 20% ethanol and finally a 40 minute wash with dH2O. Then, just prior to running the experiment, a bottle containing EZ-rich defined medium (EZRDM) is hooked up to the platform and pumped through all the tubing to remove the water and replace it with media. While this is taking place, the chip is loaded as described below. Once the fresh media has washed out the water, the media used for wash is removed and the flask containing the growth media is attached to the setup.

At the beginning of an experiment, the 500 ml baffled flask containing 200 ml of pre-warmed media is inoculated 1:10,000 of liquid culture. It is then immediately placed into the incubator where it is both maintained at 37°C and actively shaken at 220 rpm. The liquid from a flask containing either fresh media or the actively growing culture is pumped through silicone tubing then into the microscope incubator where it is connected to the mother machine via blunt-end needles. In this path, there is a small, sealed chamber that acts to remove bubbles and is also a vessel in which the OD is continuously measured. A different set of flask and pumps are used to flow fresh media when we need to monitor the cells that exit from stationary phase. The switch between the culture and the fresh media is handled with pinch-valves setup that minimizes any delay between the two conditions and also avoids any possible contamination in the fresh media from the culture (see Supplementary Information section 1).

Microscopy and image acquisition: We have custom-designed a microscope for the fast acquisition needed for the high-throughput imaging of mother machine. We replaced the turrets that house the dichroic mirror and emission filter to have a single quad band dichroic mirror for all the excitation and have a fast emission filter wheel for all the emission filters. This avoids the lags from the slow movement of the turret and improved our speed of acquisition tremendously. We then used an air objective with high NA (Apochromat, 40x, 0.95 NA) to acquire the images, which made the entire time for stage movement comparable to exposure time, allowing us to scan the entire device in less than 5 minutes. Images were acquired with a sCMOS camera (ANDOR Zyla 4.2), which allowed us to have fast frame-rate with very high QE (84%). We used a LED lamp as the white-light source for the phase contrast imaging and the Spectra-X light engine LED excitation source (Lumencor) for fluorescence imaging. Using these settings we acquired a total of 705 field of views every 5 min, allowing us to track cells in 131,072 trenches over time. For phase contrast imaging, we switched to a high magnification apodized phase contrast objective (100x oil NA 1.3, PH3), that allowed us to get high-contrast images of cells in mother machine. We sampled 85 field of views in 1 min using this oil objective allowing us to image a total of 3,500 trenches. For long acquisition it is important to keep the entire sample in perfect focus, and so the focal drift was controlled via the Nikon Perfect Focus system. The entire setup of flow-switch and the Nikon Ti inverted microscope was housed in a temperature-controlled incubator (OKO lab). We have used the Nikon Elements software for the acquisition control and to create position list using a grid structure. The fluorescent colors were ordered according to their order in the filter wheel, and the travel of the stage along the position list was optimized to get the fastest possible scanning of the entire chip. The PSF was always kept in 'on' option for fast scanning. The data were saved locally in ND2 format to improve writing and saving speed and eventually extracted for analysis into single TIFF files using a custom-made ND2extractor Python script.

Data processing: segmentation and single-cell tracking: We have developed an image-processing pipelines for processing the large volume of high-throughput data collected per experiment (~1.5 TB/ experiment). A multi-core extraction algorithm was used to extract single TIFFs from the ND2 file and organize them into folders for each field of view (FOV). We then proceeded to analyze the stack of single TIFFs for each FOV over time. The pipeline for the analysis involves four major sections: image segmentation, data extraction, single-cell tracking, and trace-cleaning. The image segmentation step involves processing the entire field of view to identify single cells and find a contour for each cell from which the intensity data is going be extracted. One major challenge for single-cell segmentation for a data along the growth-curve is that cells continuously change their size and shape along the growth-curve. To address this, we have developed a custom build segmentation algorithm that is more flexible for variable cell sizes. We first adjust contrast across all the frames of the time-lapse image stack to correct for changes in intensity of segmentation marker/phase contrast for every individual the TIFF files. Then we perform background subtraction intensity using a rolling ball algorithm. The background subtracted images were processed with a combination of global and local thresholding to create binary masks for cells from background and use a marker-based watershed algorithm to separate all the binary masks into masks single cells in a reliable manner. The segmentation algorithms are different for the

fluorescent images and phase contrast images. After the segmentation, we extract the fluorescence intensity properties and shape properties for each connected component from the list of masks.

The next step is to track single masks over time to get time-lapse data. An individual FOV has ~230 trenches with ~8 cells each. Therefore, in order to track single cells over time, we have to assign the ~1300 binary masks to their corresponding masks in different time-points. This is a massive task if to be done by the traditional frame-by-frame nearest neighbor assignment. To address this challenge, we have developed a novel clustering algorithm that cluster all the cells in a single trench over the entire duration of the experiment and then assign the top one in each frame as the mother cell. Specifically, we use DBSCAN clustering to cluster the data into lineages from individual trenches and then sort the data to get the top cell in each trench and assign all of their properties to mother-cell properties. The segmentation algorithm is not perfect, so we define criteria to help filter out data that is un-physical. The ratio of the division length and birth length should be 0.5, so we filter out any division interval where the length at birth over the length at the preceding division differs from 0.5 by more than 20%, The single-cell traces of the different properties of interest were further cleaned to remove unnatural trends using the reference marker intensity traces.

AUTHOR CONTRIBUTION

SB, EL, and JP designed the study. SB, EL, CJB designed and developed the platform. SB, SJC, and EL designed the microfluidic devices and SJC and EL constructed the devices. SB, EL, and SJC performed the mother-machine experiments. CJB and BO helped with the MACS experiments. SB and CJB developed the image analysis platform. SB, CJB, EL, and JP wrote the paper.

ACKNOWLEDGMENT

We thank Suyang Wan for her python code for extracting TIFF files from the ND2 files. We thank Nathan Lord for the master of the first mother machine we used. We thank Po-Yi and Ariel Amir for the discussion of the size regulation analysis. Rich Losick's lab and David Rudner's lab provided the strains and necessary protocols for the *B. subtilis* experiments. We thank Pavel Gorelik and Ofer Mazor at the HMS Research Instrumentation Core Facility for assistance in instrument design and fabrication. The microfabrication involved in this work was performed in part at the in part at the Harvard Medical School Microfluidics Facility and Center for Nanoscale Systems (CNS), a member of the National Nanotechnology Coordinated Infrastructure Network (NNCI), which is supported by the National Science Foundation under NSF award no. 1541959. CNS is part of Harvard University.

CODE AVAILABILITY

All scripts and code analyses necessary to segment the raw images and to perform subsequent analysis are available from corresponding author (SB and JP) upon reasonable request.

DATA AVAILABILITY

The data generated and/or analyzed during the current study are available from corresponding author (SB and JP) upon reasonable request.

REFERENCE

1. Koch, A. L. The Adaptive Responses of Escherichia coli to a Feast and Famine Existence. *Adv. Microb. Physiol.* **6**, 147–217 (1971).

2. Morita, R. Y. The starvation-survival state of microorganisms in nature and its relationship to the bioavailable energy. *Experientia* **46**, 813–817 (1990).

3. Novitsky, J. A. & Morita, R. Y. Possible strategy for the survival of marine bacteria under starvation conditions. *Mar. Biol.* **48**, 289–295 (1978).

4. Roszak, D. B. & Colwell, R. R. Survival strategies of bacteria in the natural environment. *Microbiol.*

Mol. Biol. Rev. **51**, 365–379 (1987).

5. Lennon, J. T. & Jones, S. E. Microbial seed banks: the ecological and evolutionary implications of dormancy. *Nat. Rev. Microbiol.* **9**, 119–130 (2011).

6. Navarro Llorens, J. M., Tormo, A. & Martínez-García, E. Stationary phase in gram-negative bacteria. *FEMS Microbiol. Rev.* **34**, 476–495 (2010).

7. Buchanan, R. E. Life Phases in a Bacterial Culture. *J. Infect. Dis.* **23**, 109–125 (1918).

8. Monod, J. The Growth of Bacterial Cultures. *Annu. Rev. Microbiol.* **3**, 371–394 (1949).

9. Manina, G., Dhar, N. & McKinney, J. D. Stress and Host Immunity Amplify Mycobacterium tuberculosis Phenotypic Heterogeneity and Induce Nongrowing Metabolically Active Forms. *Cell Host Microbe* **17**, 32–46 (2015).

10. Bódi, Z. *et al.* Phenotypic heterogeneity promotes adaptive evolution. *PLOS Biol.* **15**, e2000644 (2017).

11. Grimbergen, A. J., Siebring, J., Solopova, A. & Kuipers, O. P. Microbial bet-hedging: the power of being different. *Curr. Opin. Microbiol.* **25**, 67–72 (2015).

12. Casadesús, J. & Low, D. A. Programmed heterogeneity: epigenetic mechanisms in bacteria. *J. Biol. Chem.* **288**, 13929–35 (2013).

13. Givskov, M., Eberl, L., Møller, S., Poulsen, L. K. & Molin, S. Responses to nutrient starvation in Pseudomonas putida KT2442: analysis of general cross-protection, cell shape, and macromolecular content. *J. Bacteriol.* **176**, 7–14 (1994).

14. Okumus, B. *et al.* Single-cell microscopy of suspension cultures using a microfluidics-assisted cell screening platform. *Nat. Protoc.* **13**, 170–194 (2017).

15. Davey, H. M. & Winson, M. K. Using flow cytometry to quantify microbial heterogeneity. *Curr. Issues Mol. Biol.* **5**, 9–15 (2003).

16. Norman, T. M., Lord, N. D., Paulsson, J. & Losick, R. Memory and modularity in cell-fate decision making. *Nature* **503**, 481–486 (2013).

17. Wang, P. *et al.* Robust Growth of Escherichia coli. *Curr. Biol.* **20**, 1099–1103 (2010).

18. Moyed, H. S. & Bertrand, K. P. hipA, a newly recognized gene of Escherichia coli K-12 that affects frequency of persistence after inhibition of murein synthesis. *J. Bacteriol.* **155**, 768–775 (1983).

19. Balaban, N. Q. *et al.* Definitions and guidelines for research on antibiotic persistence. *Nat. Rev. Microbiol.* **17**, 441–448 (2019).

20. Ullman, G. *et al.* High-throughput gene expression analysis at the level of single proteins using a microfluidic turbidostat and automated cell tracking. *Philos. Trans. R. Soc. Lond. B. Biol. Sci.* **368**, 20120025 (2013).

21. Sturm, A. & Dworkin, J. Phenotypic Diversity as a Mechanism to Exit Cellular Dormancy. *Curr. Biol.* **25**, 2272–2277 (2015).

22. Dworkin, J. & Shah, I. M. Exit from dormancy in microbial organisms. *Nat. Rev. Microbiol.* **8**, 890–896 (2010).

23. Mutlu, A. *et al.* Phenotypic memory in Bacillus subtilis links dormancy entry and exit by a spore quantity-quality tradeoff. *Nat. Commun.* **9**, (2018).

24. Gefen, O., Fridman, O., Ronin, I. & Balaban, N. Q. Direct observation of single stationary-phase bacteria reveals a surprisingly long period of constant protein production activity. *Proc. Natl. Acad. Sci.* **111**, 556–561 (2013).

25. Neidhardt, F. C., Bloch, P. L. & Smith, D. F. Culture medium for enterobacteria. *J. Bacteriol.* **119**, 736–47 (1974).

26. Konopka, M. C. *et al.* Cytoplasmic protein mobility in osmotically stressed Escherichia coli. *J. Bacteriol.* **91**, 231–237 (2009).

27. Barns, K. J. & Weisshaar, J. C. Real-time attack of LL-37 on single Bacillus subtilis cells. *Biochim. Biophys. Acta* **1828**, 1511–20 (2013).

28. Okumus, B. *et al.* Mechanical slowing-down of cytoplasmic diffusion allows in vivo counting of proteins in individual cells. *Nat. Commun.* **7**, 11641 (2016).

29. Amir, A. Cell Size Regulation in Bacteria. *Phys. Rev. Lett.* **112**, 208102 (2014).

30. Logsdon, M. M. *et al.* A Parallel Adder Coordinates Mycobacterial Cell-Cycle Progression and Cell-Size Homeostasis in the Context of Asymmetric Growth and Organization. *Curr. Biol.* **27**, 3367-3374.e7 (2017).

31. Eun, Y.-J. *et al.* Archaeal cells share common size control with bacteria despite noisier growth and division. *Nat. Microbiol.* **3**, 148–154 (2018).

32. Cadart, C. *et al.* Size control in mammalian cells involves modulation of both growth rate and cell cycle duration. *Nat. Commun.* **9**, 3275 (2018).

33. Chandler-Brown, D., Schmoller, K. M., Winetraub, Y. & Skotheim, J. M. The Adder Phenomenon Emerges from Independent Control of Pre- and Post-Start Phases of the Budding Yeast Cell Cycle. *Curr. Biol.* **27**, 2774-2783.e3 (2017).

34. Taheri-Araghi, S. *et al.* Cell-size control and homeostasis in bacteria. *Curr. Biol.* **25**, 385–391 (2015).

35. Campos, M. *et al.* A Constant Size Extension Drives Bacterial Cell Size Homeostasis. *Cell* **159**, 1433–1446 (2014).

36. Zaritsky, A. & Helmstetter, C. E. Rate maintenance of cell division in Escherichia coli B/r: analysis of a simple nutritional shift-down. *J. Bacteriol.* **174**, 8152–5 (1992).

37. Gonzalez-Pastor, J. E., Hobbs, E. C. & Losick, R. Cannibalism by Sporulating Bacteria. *Science (80-.).* **301**, 510–513 (2003).

38. Chien, A.-C., Hill, N. S. & Levin, P. A. Cell size control in bacteria. *Curr. Biol.* **22**, R340-9 (2012).

39. Amodeo, A. A. & Skotheim, J. M. Cell-Size Control. *Cold Spring Harb. Perspect. Biol.* **8**, a019083 (2016).

40. Si, F. *et al.* Mechanistic Origin of Cell-Size Control and Homeostasis in Bacteria. *Curr. Biol.* **29**, 1760-1770.e7 (2019).

41. Sekar, K. *et al.* Synthesis and degradation of FtsZ quantitatively predict the first cell division in starved bacteria. *Mol. Syst. Biol.* **14**, 1–14 (2018).

42. Balaban, N. Q., Merrin, J., Chait, R., Kowalik, L. & Leibler, S. Bacterial persistence as a phenotypic switch. *Science* **305**, 1622–5 (2004).

43. Kohanski, M. A., Dwyer, D. J. & Collins, J. J. How antibiotics kill bacteria: from targets to networks. *Nat. Rev. Microbiol.* **8**, 423–35 (2010).

44. Jørgensen, B. B. & Boetius, A. Feast and famine — microbial life in the deep-sea bed. *Nat. Rev. Microbiol.* **5**, 770–781 (2007).

45. Veening, J.-W., Smits, W. K. & Kuipers, O. P. Bistability, Epigenetics, and Bet-Hedging in Bacteria. *Annu. Rev. Microbiol.* **62**, 193–210 (2008).

46. Ackermann, M. A functional perspective on phenotypic heterogeneity in microorganisms. *Nat. Rev. Microbiol.* **13**, 497–508 (2015).

47. Jõers, A. & Tenson, T. Growth resumption from stationary phase reveals memory in Escherichia coli cultures. *Sci. Rep.* **6**, 24055 (2016).

48. Si, F. *et al.* Mechanistic origin of cell-size control and homeostasis in bacteria. *bioRxiv* 478818 (2018). doi:10.1101/478818

49. Ronneau, S. & Helaine, S. Clarifying the Link between Toxin–Antitoxin Modules and Bacterial Persistence. *J. Mol. Biol.* (2019). doi:10.1016/j.jmb.2019.03.019

50. Baba, T. *et al.* Construction of Escherichia coli K-12 in-frame, single-gene knockout mutants: the Keio collection. *Mol. Syst. Biol.* **2**, 2006.0008 (2006).

51. Zaslaver, A. *et al.* A comprehensive library of fluorescent transcriptional reporters for Escherichia coli. *Nat. Methods* **3**, 623–628 (2006).